



Experimental and Theoretical Verification of WO₃ Based Nanocomposites for Their Application as Efficient Photo Catalyst for Treatment of Industrial Wastewater

Maria Ashraf¹ · Tahir Iqbal¹ · Arslan Masood¹ · Najat Masood^{2,3} · Faiza I. A. Abdella² · Walaa I. El-Sofany^{2,4} · Sami M. Magam^{3,5} · Mubeen Arif⁶ · Muhammad Salim Mansha¹

Received: 29 March 2023 / Accepted: 6 May 2023 / Published online: 16 May 2023

© The Author(s), under exclusive licence to Springer Science+Business Media, LLC, part of Springer Nature 2023

Abstract

In this research work, CuS and WO₃ nanoparticles were synthesized by a simple, facile and effective hydrothermal method followed by the fabrication of nanocomposites of 10, 12 & 14% CuS:WO₃. The prepared samples were characterized by various characterization techniques including X-ray diffraction (XRD), UV–Visible (UV–vis), photoluminescence (PL), Energy dispersive X-ray (EDX) and field emission scanning electron microscopy (FE-SEM) for the confirmation and investigation of fabricated nanocomposites. The particle size of fabricated WO₃ was 46.01 nm which was reduced to 37.14 nm for 14% CuS:WO₃ sample. Additionally, UV visible and PL analysis confirmed the suppression of band gap (2.61 to 2.25 eV) and photogenerated electron/hole pair respectively. Photocatalytic activity of as prepared nanocomposites was investigated under visible light irradiation against rhodamine B (RhB) dye. Quite interestingly, the photodegradation efficiency of 14% CuS-WO₃ is 94.91% which is much higher as compared to pure WO₃ which attributes to the smaller particle size and bad gap energy which enables the efficient utilization of visible light leading to the generation of reactive species. Reusability experiments confirmed the photostability of samples and pH tests have also been conducted to investigate the optimum pH for degradation reaction. For investigation of complete mineralization of RhB dye from contaminated water, TOC analysis

Maria Ashraf, Tahir Iqbal and Arslan Masood have equally contributed to this article.

✉ Tahir Iqbal
tahir.awan@uog.edu.pk

✉ Arslan Masood
arslanmasood0043@gmail.com

✉ Najat Masood
ne.ebrahim@uoh.edu.sa

¹ Department of Physics, Faculty of Science, University of Gujrat, Hafiz Hayat Campus, Gujrat 50700, Pakistan

² Department of Chemistry, Faculty of Science, University of Ha'il, Hail, Saudi Arabia

³ Department of Marine Chemistry and Pollution, Faculty of Marine Science and Environment, Hodeidah University, Hodeidah, Yemen

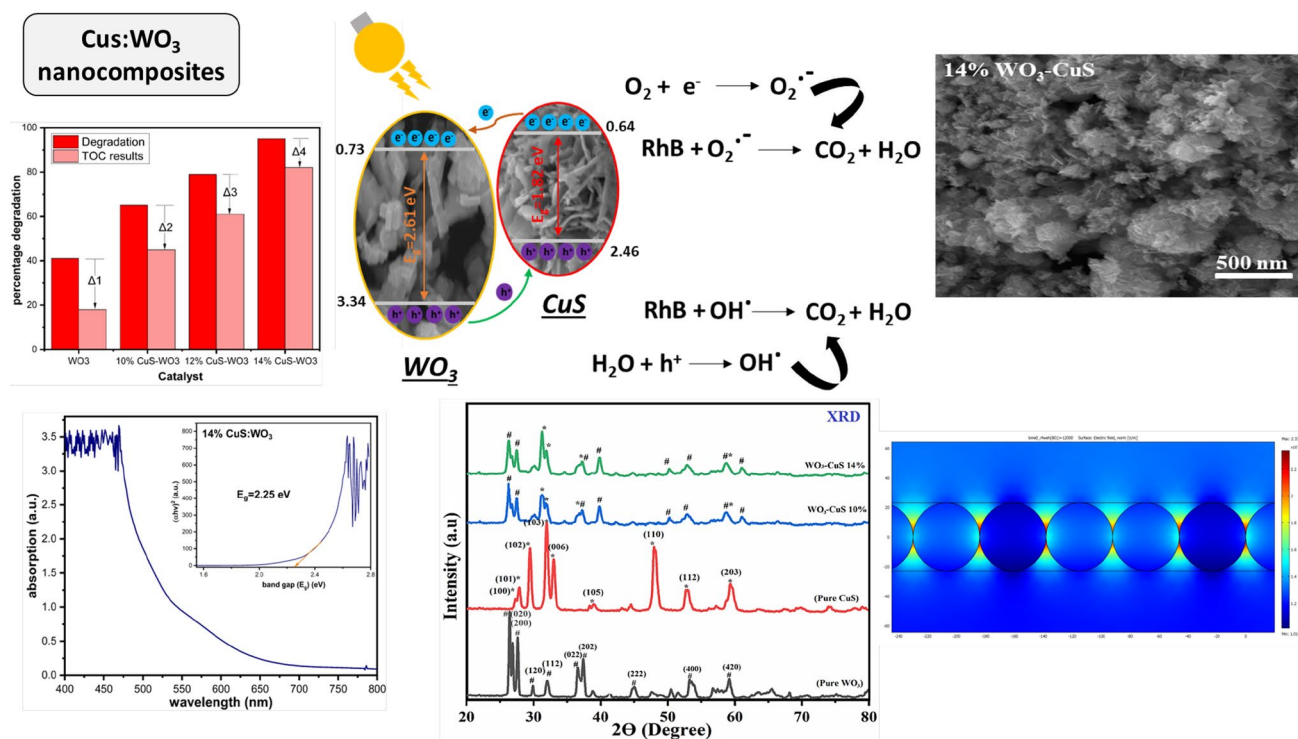
⁴ Photochemistry Department, Chemical Industries Research Institute, National Research Centre, Scopus Affiliation ID 60014618, 33 EL Buhouth St., Dokki, Giza 12622, Egypt

⁵ Basic Science Department, Preparatory Year, University of Ha'il, Hail 1560, Saudi Arabia

⁶ Department of Chemistry, Faculty of Science, University of Gujrat, Hafiz Hayat Campus, Gujrat 50700, Pakistan

has been conducted. Additionally, RF module of COMOSL Multiphysics 5.3a has been used to simulate a 2D model to correlated the experiment with the theoretical results for better understanding.

Graphical Abstract



Keywords Hydrothermal approach · CuS-WO₃ · RhB · Nanocomposites · Photocatalysis

1 Introduction

In recent few years, the contaminated water due to the dyes, pesticides and other contaminants drugs has gained significant attention owing to their carcinogenic effects on human beings and the environment. Several emerging countries rely heavily on their textile industry for economic growth. Predominantly, the raw materials needed for this sector includes synthetic dyes. There are approximately 10,000 distinct synthetic dyes and more than 700,000 tons of these dyes are produced annually out of which up to 200,000 tons of synthetic dyes are released into the environment without any treatment. The pollution created by the industrial and commercial sectors is rising. Organic dyes are hazardous and non-biodegradable, causing contamination in the textile, cosmetic, and food sectors [1, 2]. The World Bank estimates that the dyeing and finishing of textiles produces between 17 and 20 percent of the industrial wastewater. Therefore, for the sustainability of the environment, treatment of dye polluted water has become a necessity. For this purpose, several conventional

and non-conventional methods have been utilized such as nano-filtration, adsorption, coagulation, ozonolysis and photocatalysis. Among these techniques, photocatalysis is used widely due to its efficiency.

The manufacture of highly ordered semiconductor photocatalyst designs has stimulated a lot of attention due to their constant growth with specific shape and accessible usage for energy and sustainability concerns [3]. Degradation rate is an effective parameter for measurement of degradation of organic contaminants from waste water. Since the last several decades, a multitude of active semiconductor photocatalysts such as metal oxide, sulfide, oxynitrides, and graphite carbon nitride have indeed been tried to introduce and used for the organic pollutants are removed in aquatic environments [4–7]. Generally, most of the metal oxides have band gap in UV region which restricts the utilization of solar spectrum as only 5% of solar light consists of UV wavelength. Tuning the band gap from UV to visible region by doping, co-doping or nano-composites to produce a visible light driven efficient photocatalyst is the main goal of scientists and researchers.

It seems essential to push significantly with catalytic materials (in visible region) in order to figure out significant energy concerns [8, 9].

Tungsten oxide (WO_3) is a reputable and crucial semiconductor catalyst among all other materials such as ZnO, TiO_2 , MoS_2 etc. due to its highly responsive nature under UV–Visible irradiance, mechanical characteristics, and excellent photostability [10, 11]. Tungsten oxide is utilized in photocatalytic and polarizing filters devices, as well as electrodes. Tungsten oxide photocatalytic performance is still limited due to fast recombination rate of charge carriers and inability of O_2 to effectively grab these electrons to produce superoxide radicals which are crucial for the degradation reaction [12]. The location of band gap is reformed by researchers for tungsten oxide through adding low band gap semiconductors to the catalyst to minimize the charge recombination and boosting the photocatalytic activity [13]. The maximum absorbance spectrum is prolonged and charge recombination rate is decreased because of the disparity in conduction and valence band energies between the two semiconductors [14]. Furthermore, it increases the yield of photogenerated electrons located in the conduction band, which aids in photocatalytic degradation. There is very little literature on CuS- WO_3 for the degradations of organic contaminants therefore, it is interesting to investigate the photocatalytic performance of said material. Due to its strong optical, electrical, and availability qualities, CuS is utilized to make a nano-composite with WO_3 .

CuS is an ideal material for renewable power absorption due to its low absorbance in the visible range and strong reflection in the near infrared range [15]. Although, WO_3 has a band gap in the range of visible light but its high charge recombination rate makes it a poor photocatalyst for the commercial scale usage. Addition of CuS may vary the band gap of material and provide trapping energy level to reduce the recombination rate which could play a positive role in the degradation of rhodamine B (RhB) dye from wastewater.

In this research work, a facile and efficient hydrothermal approach has been used to synthesize pure CuS and WO_3 nanoparticles. Moreover, CuS- WO_3 nanocomposites were synthesized for 10%, 12% and 14% CuS concentration. Variation in structural, optical and morphological characteristics were studied by XRD, SEM, EDX, UV, PL etc. Photocatalytic degradation of rhodamine B (RhB) dye was examined in the presence of synthesized nanocomposite. Effect of pH was also investigated on the degradation of RhB dye using the best photocatalyst among all the synthesized sample. Total organic carbon analysis has provided valuable information about the complete mineralization percentage of the dye. To check the photostability of the synthesized nanocomposites, the degradation of RhB dye for 6 cycles has been carried out. RF module of COMSOL Multiphysics 5.3 has been used to mimic a 2D model of the experimental

procedure and the effect of concentration of CuS in WO_3 on the absorption of visible to near infrared light has been examined over time to estimate the photocatalytic performance of the nanocomposites.

2 Materials and Methods

Copper sulphate pentahydrate ($\text{CuSO}_4 \cdot 5\text{H}_2\text{O}$) sodium thiosulfate 200 mL deionized water, 50 mL isopropanol, CTAB ($\text{C}_{19}\text{H}_{42}\text{BrN}$) cetrimonium bromide Sodium tungstate dihydrate ($\text{Na}_2\text{WO}_4 \cdot 2\text{H}_2\text{O}$), sodium chloride (NaCl), sulfuric acid (H_2SO_4), hydrochloric acid (HCL), ethanol, and deionized After processing, all reagents were utilized.

2.1 Synthesis of Photocatalyst CuS, WO_3 and Composite

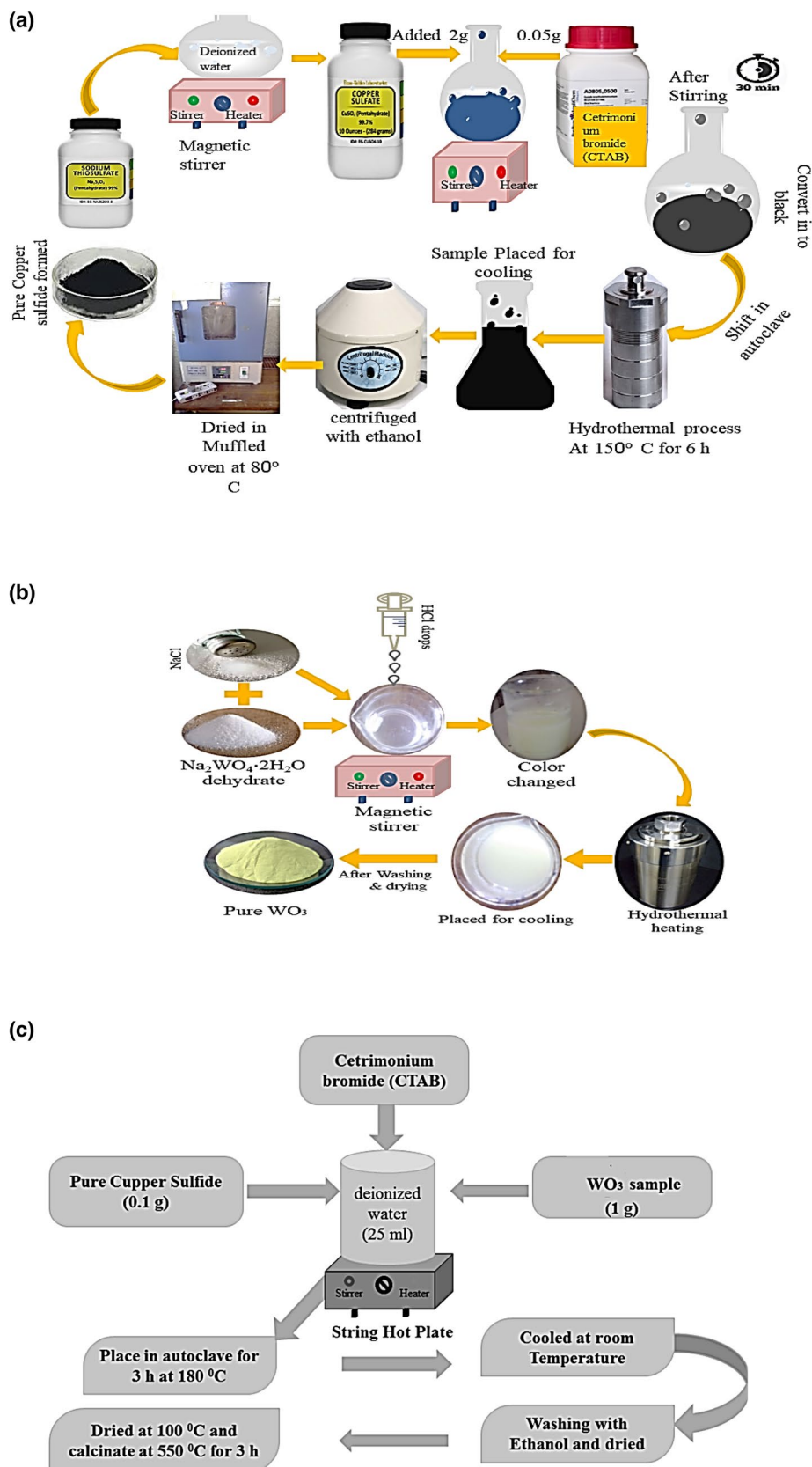
To synthesize copper sulfide, mix 2 g sodium thiosulfate in 100 mL distilled water and agitate for 20 min to create a moisturizer mixture that contains thiosulfate ions ($\text{S}_2\text{O}_3^{2-}$), which act as an oxidizing agent. While stirring, 2 g copper sulphate was given to the produced serum, resulting to cupric ions (Cu^{2+}) in the mixture, acted as an oxidant that initiated an oxidation process in the compounds. When copper sulphate was exposed to sodium thiosulfate serum, it became colorless and eventually black. To lower the surface tension of the components, 0.05 g of Cetrimonium bromide was included in the mixture as an agitator. The hydrothermal method has been utilized to create CuS, which entailed putting a solution inside an autoclave at 150 °C Celsius for 6 h. After that, the sample was allowed to recede to ambient temperature. After synthesis let it dry in an 80 °C Muffled oven. Figure 1a depicts the manufacture of pure dried black copper sulfide [16].

$\text{Na}_2\text{WO}_4 \cdot 2\text{H}_2\text{O}$ 0.01 mol and 0.06 mol pure sodium chloride were diffused in 30 ml of distilled water in a clean beaker shown in the Fig. 1b. The reaction was taken place using autoclave for 12 h at 180 °C. the reaction mixture is allowed to cool getting yellow precipitates. Pure precipitates are obtained by multiple washing with cold deionized water, ethanol and let it dry in an oven at 120 °C. The weight percentages of CuS added WO_3 were calculated: 10, 12 and 14%. Solutions of Tungstic acid (0.008 mol), CTAB (0.002 mol) in water were set into an autoclave machine and the process followed is shown in Fig. 1c. [17].

2.2 Characterization of Photocatalysts

The required samples estimated for the enhancement of photocatalytic properties after they have been synthesized. The structural parameters were determined by the “Bruker D8 X-ray Diffraction technique with Cu-k x-ray

Fig. 1 a CuS preparation with active $\text{Na}_2\text{S}_2\text{O}_3$ and copper sulphate. **b** Preparation of WO_3 by sodium chloride and Sodium tungstate di-hydrate reaction. **c** Preparation of WO_3 composite with CuS by Sodium tungstate di-hydrate and NaCl



source = (1.541874)'' range of 20–80 degrees. The morphological analysis of samples has been done with “TESCAN MAIA3 Field emission Scanning Electron Microscopy.” Photoluminescence behavior was observed with photoluminescence (FP-8200 Spectrofluorometer JASCO) giving emission spectra between 420 and 550 nm. At last, the photocatalytic activity was addressed using ‘V-730 Ultraviolet–Visible Spectroscopy’ [18].

3 Results and Discussion

3.1 Morphology and Elemental Analysis

The morphological characteristics and shape of the photocatalysts have been characterized by elemental analysis and SEM data as shown in Fig. 2a & b. In present study, classified flower-shaped CuS and WO₃ photocatalysts nanorods are more conducive to photoelectron hole pair expansion and separation. Thus, synthetic flowers such as CuS and WO₃ nanorods are considered as optimistic probes for photocatalytic activity. Sharp edges for WO₃ nano-rods are observed with 10% concentration of CuS and overall, its morphology is needlelike. Petals of CuS is specific for pronounce and efficient growth of WO₃ nanostructures. Geometrical morphology is determined by 14% and it was noticed that the synthesized Nano probes are having sharp edges. The tiny nanoflowers with nano-petals increase the area of absorbance meant for RhB mortification which suggests that 14% CuS sample has an immense surface morphology, supplementary reactive sites and increased photocatalytic behavior [19]. Energy dispersive Xray spectroscopy (EDAX) of 10 and 14% CuS:WO₃ nanocomposites in Fig. 2(b) verified the occurrence of peaks corresponding to W, Cu, S and O atoms. The weight and molarity percentage of each species is mentioned in the inset of EDX graphs in Fig. 2b.

3.2 X-Ray diffraction (XRD)

XRD helped measuring the phase, dimensions, and morphology of WO₃ composite with CuS representatives as shown in Fig. 3. XRD Micrograph manifest that pure WO₃ subdue plans (020), (200), (120), (112), (020) (202) (222) (400) and (420.0) with corresponding angles, 25.3°, 25.9°, 28.8°, 33.2°, 36.2°, 37.2°, 45.1°, 42.9° and 57.4° respectively. WO₃ sample bearing the monoclinic geometry and its JCPDS no. is 03–1823. The sample showed geometrical parameters $\alpha = 90^\circ$, $\beta = 89.93^\circ$ $\gamma = 90^\circ$ and a, b and c are 7.274 (Å), 7.501 (Å) and 3.824 (Å) respectively while the density is 7.380 g/cm³. Nearly same crystallographic features were observed for pure WO₃, 10, 12 and 14% CuS composites [20]. With reference to JCPDS file (06–0464) CuS is

hexagonal with a = 3.796 Å and c = 16.209 Å furthermore, composites having 10% CuS are changing the parameters of x-ray for tungsten WO₃. (#) and (*) are representation for the peaks of CuS and WO₃ planes respectively as shown in Fig. 4. Single WO₃ and CuS peaks are identified for the composites of CuS and WO₃. Change in concentration of CuS is not affecting the WO₃ planes but inversely varying the concentration. 10% composites are giving less intense peaks of CuS than 14%. Furthermore the Scherer’s formula (Eq. 1) was used to verify the size of crystal by (101) peak. [21]. Table 1 shows the lattice parameters and Scherrer size of nanocomposites.

$$D = \frac{0.9\lambda}{\beta \cos \theta} \quad (1)$$

Furthermore, the peaks of the diffraction planes (002), (101) and (100) have shifted downwards. The peaks denoted by (*#) describes the mixing of CuS (200) and (202) peaks transferring to lower values increased concentration of copper sulfide.

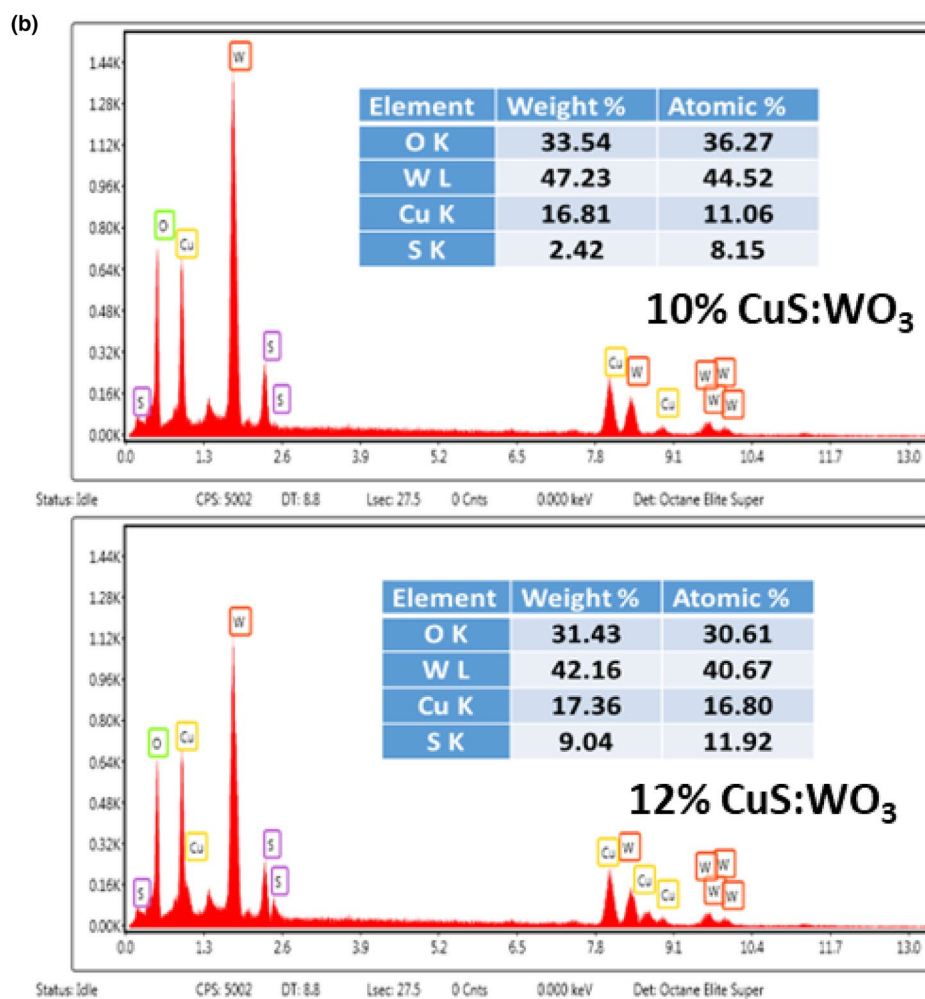
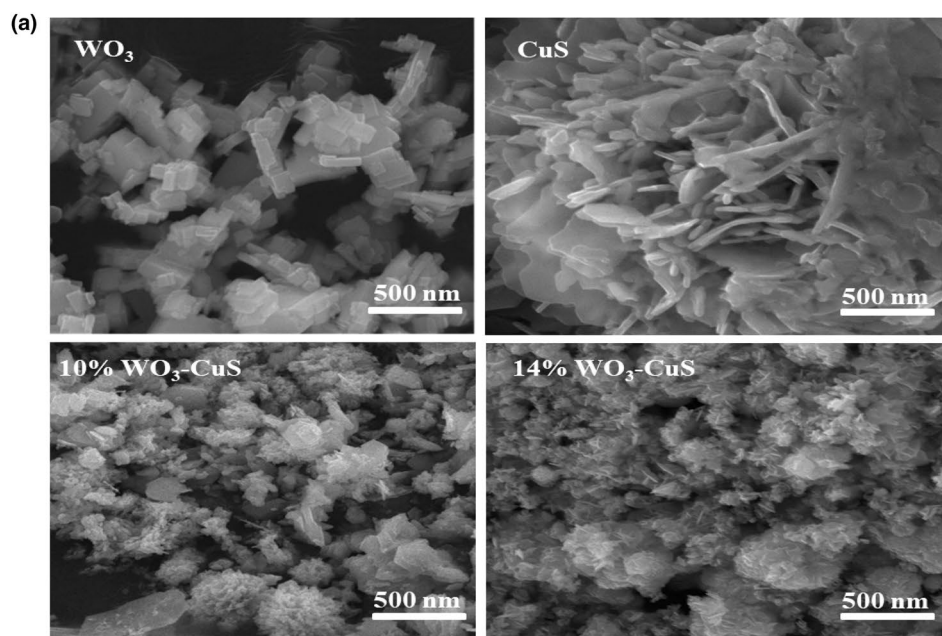
3.3 Optical Absorption Studies

The light-absorbing properties of copper-sulfide, Tungsten-trioxide and WO₃-CuS were inspected by photo-catalysts using UV–Vis analysis, shown in spectroscopy and spectral features Fig. 4. Absorption for synthesized CuS, WO₃, 10% and 14% CuS:WO₃ were analyzed and the bandgap (BG) values of 1.82, 2.61, 2.47 and 2.25 eV respectively, along with the overview of visible light absorption increasing the ion capacity for CuS:WO₃. It was observed that by the addition of copper-sulfide material absorption interchanges in visible range, due to 14% copper-sulfide in the sample of tungsten-trioxide. Its Tauc’s plot demonstrated the decrease in energy by alteration in band gap (BG). This behavior confirms that CuS doped WO₃ material is appreciated for the optimized results of optical properties. This decrease in band gap can efficiently enhance the photo-catalysis of prepared samples.

3.4 Photoluminescence Measurements

Further, PL spectroscopy has been utilized to study the optical parameters, reunion rate of electron–hole pairs produced under UV light for pure WO₃ and its composites with CuS, shown in Fig. 5. This study was achieved at 400 nm excitation wavelength. It was seen pure WO₃ gives the emission at 464 nm and 10% probe shows that the intensity peak shifts downward carrying immense gap with increased wavelength, 464 nm. Introduction of 14% CuS will incorporate new trapping points, decrease of the intensity with

Fig. 2 **a** SEM images of pure WO_3 , flower like CuS and their nanocomposites. **b** EDX analysis of 10% and 14% WO_3 Composites with CuS along with molar and weight percentage



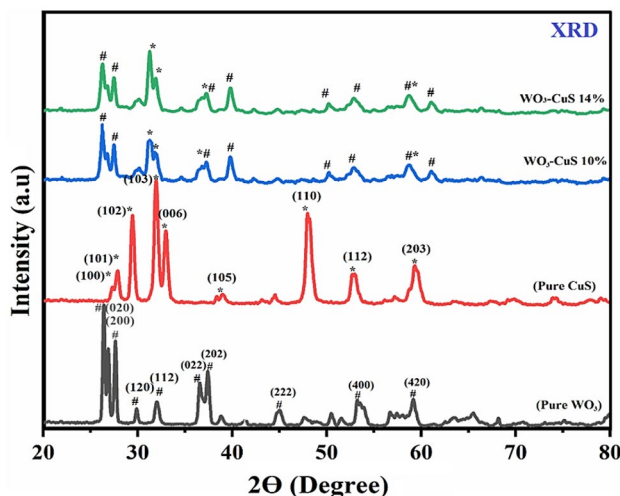


Fig. 3 XRD Pattern of pure WO_3 , CuS and respective nanocomposites

bathochromic shift of wavelength [22]. In addition to this, photoluminescence peaks are relevant to the suppression of photo-generated electron–hole pair reunion [23] which is ultimately beneficial for improving photocatalytic performance of nanomaterial.

4 Photo-Catalytic Degradation Studies

The photo-catalytic degradation of RhB has been characterized in the visible light for RhB contamination to understand the photo catalytic efficiency of synthesized photo catalysts as shown in Fig. 6. A 300W tungsten-halogen lamp was used to provide visible light irradiation. The wavelength extent of light source was greater than 400 nm and usually the distance of 20 cm is kept between the sample and lamp, a 250 ml of dye solution of known amount was added to photo-catalyst. Earlier to light contamination, the magnetically suspension was mixed in the dark to create RhB equilibrium of the photo-catalyst [18]. 4 ml of aliquots were composed at regular intervals and the photo-catalyst was cleared by adaptation through a 0.45 mm membrane Alter (Pall Corporation) during irradiation. A Shimadzu UV-2450 UV–Vis spectrophotometer was used to determine the RhB concentration at dissimilar time intermission at its absorption wavelength characteristic viz., 554 nm [23]. A brief comparison of current work with the recent literature has been shown in Table 2.

4.1 Mechanism of Photo-Catalytic Degradation

Photo-catalytic degradation mechanism of RhB is shown using $\text{CuS}:\text{WO}_3$ catalyst. The electronegativity of CuS and

WO_3 is 5.29 and 6.59 eV respectively [30]. The measured valence band (VB) and conduction band (CB) of CuS is 2.46 and 0.64 eV, whereas VB and CB of WO_3 is 3.34 and 0.74 eV, respectively. The value of the CB for copper sulfide is more negative as compared to WO_3 [30]. Consequently, the photo-induced prompted electron movement from conduction band of CuS to WO_3 and simultaneously, there is an exchange of the hole from the valence band of WO_3 to CuS. Hence, there is a decrease in electron–hole recombination and it prompts an expansion in the interfacial charge movement responses for the degradation of adsorbed particles of dye. Solution of rhodamine B (RhB) in distilled water, placed in the photo-catalytic reactor and 4 ml of sample was separated out at each 20 min interval obtaining UV–Vis spectra [31]. This study is actually meant to study the deprivation rate of the nano probes as shown in Fig. 6. The adsorption equilibrium of catalyst and dye solution was obtained to study the fabricated samples with RhB solution in dark for half an hour as shown in Fig. 9. In case of pure sample, when the contaminant model has been agitated using catalyst, nearly 1% adsorption was observed and showed bathochromic shift for 10% WO_3 and 14% CuS [32]. This increased adsorption is the outcome of the enhanced surface area, more points available for reaction which further enhancing the degrading effectiveness. The photo-catalytic efficiency of the CuS composites with WO_3 was investigated through photo degradation of pollutant RhB [33]. The deterioration rate of catalyst seemed to increase with increased portion of CuS in comparison to pure WO_3 . The absorption of 14 percent CuS mixture clearly revealed the increased degradation depicted in Fig. 6b. The maximum effectiveness was observed for 14% CuS composite. The accessed photo-catalysis is because of more active sites which further affect bandgap and electron–hole pair reunion rate [34, 35]. For investigation of effectiveness of the samples is determined by following formula (Eq. 2).

$$\text{Degradation (\%)} = (C/C_o) \times 100 \quad (2)$$

Above mentioned formula, C_o and C represents the initial and final concentration of the solution respectively. RhB is merely degraded without catalyst and it manifest that RhB is very stable. However, by adding 10 mg of prepared catalyst (WO_3) to aqueous solution, about 38% dye is degraded in 140 min as shown in Fig. 6a & c. Furthermore, proficiency of this process has heightened by increasing in the copper- sulfide ratio in tungsten trioxide. Electrons lying in valance band of photo-catalyst get excited by irradiating with a threshold frequency light and shifted to the CB. Meanwhile, the equal number of holes are there in the VB of WO_3 and CuS are the scavengers for electrons and holes, so recombination ratio has decreased [36]. The plausible oxidation reduction processes are show below.

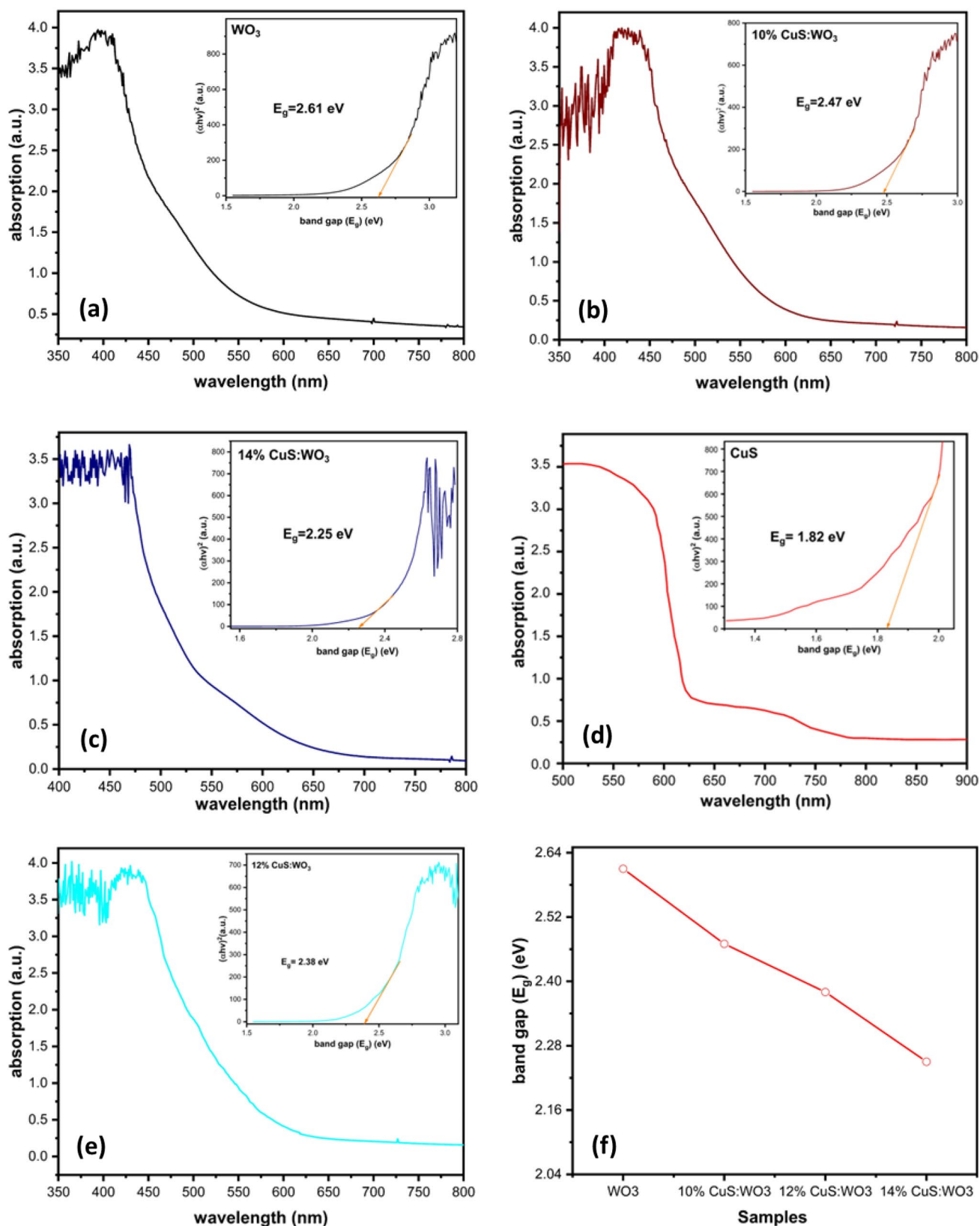
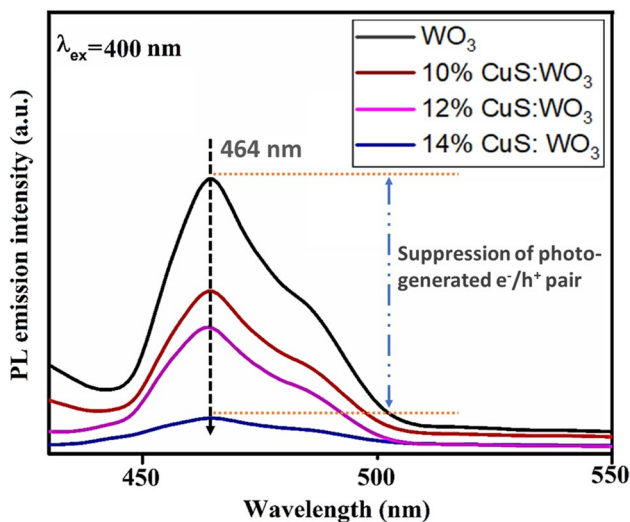
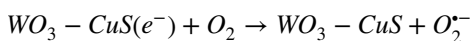
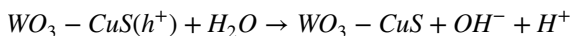
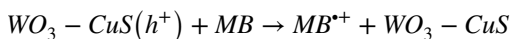
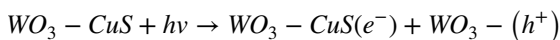


Fig. 4 UV-vis spectrum and Tauc plot of **a** WO_3 , **b** 10% CuS:WO₃, **c** 14% CuS:WO₃, **d** CuS, **e** 12% CuS:WO₃ and **f** the comparison of variation in band gap with increasing concentration of CuS in WO_3

Table 1 Lattice parameters and Scherrer size of fabricated nanocomposites

Sample	Lattice parameters (Å)			Crystallite size (nm)
	a	b	c	
WO ₃	7.274	7.501	3.824	46.01
CuS	3.976	3.976	16.209	31.62
10% CuS:WO ₃	7.252	7.496	3.816	42.37
14% CuS:WO ₃	7.545	7.488	3.811	37.14

**Fig. 5** PL Emission spectrum of WO₃ and its composite materials

14% CuS nanoprobe catalyst on reaction with water is generating hydroxyl radicals and H⁺. Fig. depicts that when catalyst is irradiated, holes are generated and the highly reactive holes are interplaying with RhB [37]. CuS:WO₃ (e⁻) combining by oxygen (O₂) forming superoxide anion radicals, hydroxyl ions while CuS-WO₃ (h⁺) are interacting with one another forming hydroxyl radicals [38]. Superficial rate constant of photo-catalysts can be determined using following formula (Eq. 3):

$$\ln(C_0/C) = (k_{app})(t) \quad (3)$$

where C is preliminary amount of dye and C₀ indicating the quantity of dye remaining at time “t”. k_{app} is apparent rate constant, the linear fitted plot between time t and ln(C₀/C) shown in Fig. 7.

4.2 Reusability and Effect of pH

Reusability and photo-stability of 14% CuS:WO₃ was measured, an effective parameter to be restrained for an efficiency of catalyst [39]. For determining recycling rate, sample was separated through magnetic field and degraded in six cycles alternatively shown in Fig. 8a. The results revealed that photo-catalytic efficacy was not reduced at the end of six cycles when 87.06% effectively was measured comparing 94.9% of the first cycle. Additionally, the effect of pH on the degradation efficiency of RhB for the best sample (14% CuS:WO₃) was investigated. In this experiment, pH of the contaminant solution is adjusted at the start of reaction and was not maintained through out the reaction. Results shown in Fig. 8b indicates that moving from acidic to basic pH, the highest degradation efficiency is obtained for 9 pH. Any further increase in pH suppresses the removal efficiency of the catalyst.

4.3 Total Organic Carbon (TOC) Analysis

TOC analysis has been conducted to check the complete mineralization of RhB dye when the contaminated dye solution is exposed to light source in the presence of synthesized photocatalyst. The results are shown in Fig. 9. The difference between degradation observed via UV–Visible spectrometer and complete mineralization percentage by TOC is denoted by Δ1, Δ2, Δ3 & Δ4 for pure WO₃, 10% CuS-WO₃, 12% CuS-WO₃ and 14% CuS-WO₃ respectively. It is observed that with the increase in CuS percentage in the nano-composite, the ability of complete degradation of RhB dye has been enhanced which is evident by the smallest value of Δ4 as compare to other values. The difference between degradation percentage and TOC results can be attributed to the fact that, it is possible for an organic dye to lose its characteristic color bond with in first few steps of the degradation reaction. The UV–Visible analysis will count the degradation when the characteristic color peak will be absent irrespective of the fact that complete mineralization is a multistep process and it is possible for the organic contaminant to possess centric benzene ring and also do not show color peak. Therefore, TOC analysis is crucial for the exact confirmation of complete degradation of pollutant. Table 3 provides a review of the critical findings of the photocatalytic performance of synthesized pure WO₃ and its nanocomposites with CuS.

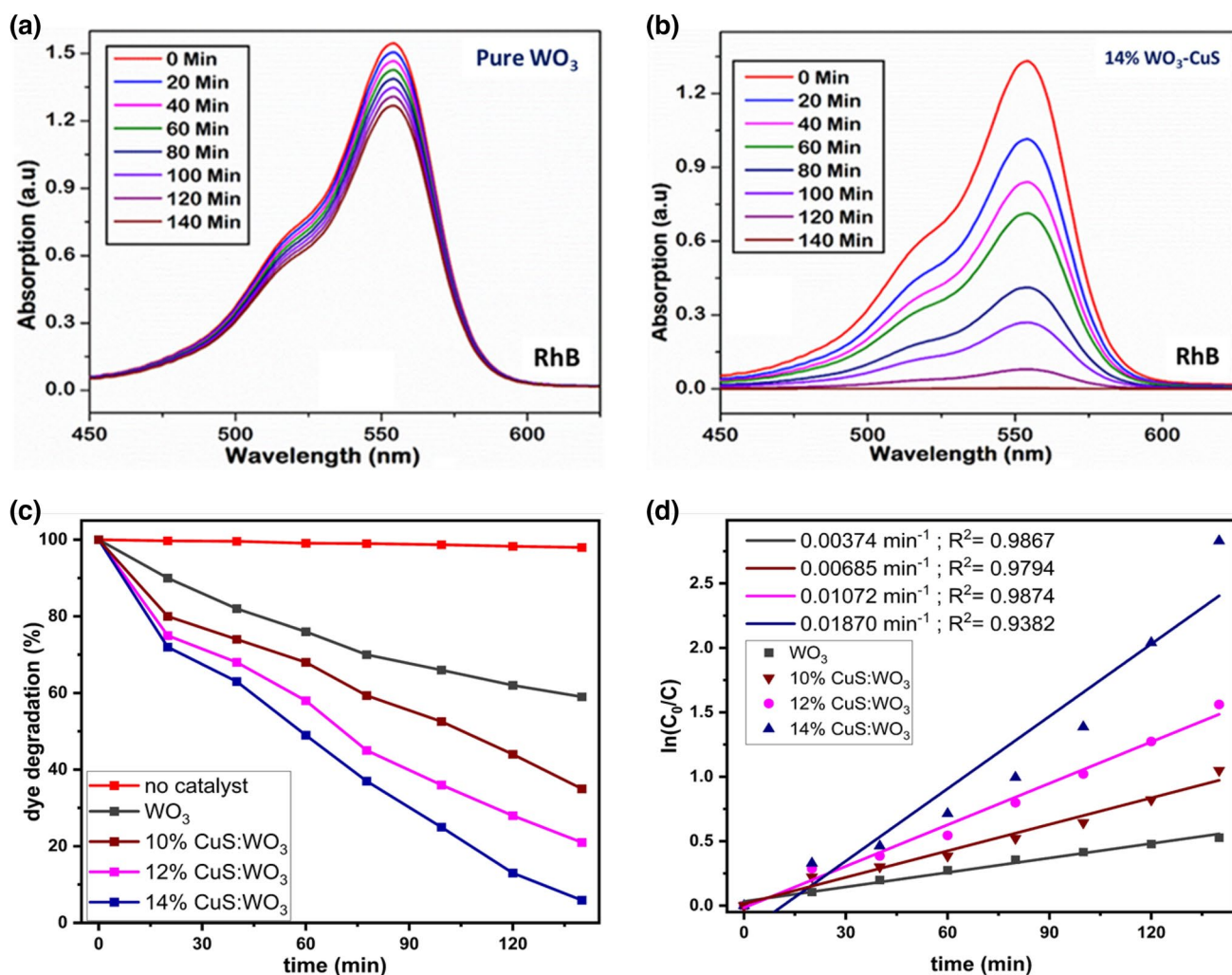


Fig. 6 a & b Depicting photocatalytic degradation of RhB dye by Pure WO_3 and 14% $\text{CuS}:\text{WO}_3$ composites respectively, c Photocatalytic removal of RhB dye in the presence of fabricated nanomaterial

and d rate constant revealing highest rate constant of 0.01870 min^{-1} for 14% $\text{CuS}:\text{WO}_3$ nanocomposite

Table 2 A comparison of present study the relevant work reported in the literature

Photocatalyst	Pollutant	Method	Light source	Result	Reference
$\text{TiO}_2\text{-WO}_3$	PNP	Soaking	500 W Xenon arc lamp	90% in 100 min	[24]
Ag-WO_3 Nanoplates	SAM	Hydrothermal method and photoreduction method	200 W Xenon arc lamp at 420–630 nm	92.5% in 5 h	[25]
Fe-WO_3	Phenol and RhB	Templet method	300 W Xe lamp	(phenol) 93% in 240 min, (RhB) 92% in 120 min	[26]
$\text{WO}_3/\text{graphene}$	MB	Hydrothermal method	500 W tungsten halogen lamp	94% in 8 h	[27]
WO_3/RGO	p-cresol	Hydrothermal method	250 W lamp	57.3% in 6 h	[28]
$\text{WO}_3@\text{SnS}_2$	RhB	Two step hydrothermal method	5 W white light LED	94.1% in 100 min	[29]
CuS-WO_3	RhB	Hydrothermal method	300 W tungsten halogen lamp at wavelength $\geq 400 \text{ nm}$	94.91% in 140 min	(Current Work)

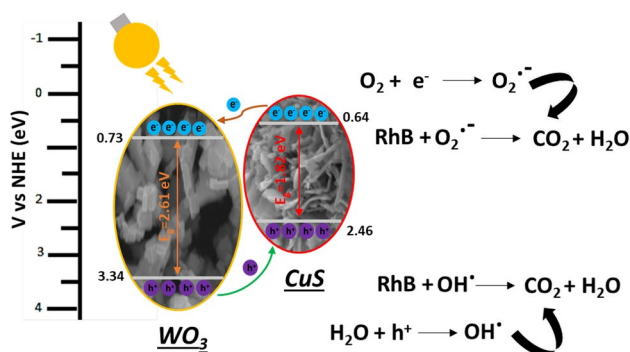


Fig. 7 Photo-catalytic Mechanism of CuS:WO₃ nanocomposites

The percentage mentioned in the table has been round off to the nearest whole number for simplicity.

4.4 COMOSL Simulation

COMSOL Multiphysics 5.3a is used to simulate the 2D model of experimental work. The schematics are shown in Fig. 10a. Different boundary conditions have been employed to mimic the experimental environment. Input port is used to excite the 2D model with UV–Visible to near infrared radiation (NIR). Scattering boundary condition (SBC) is used to ensure that the radiations are effectively dispersed. Periodic boundary conditions (PBC) are used on the right and left side of the model whereas continuous boundary conditions (CBC) are used on the inner boundaries of the model. The equations of these boundary conditions are given below (Eq. 4–7).

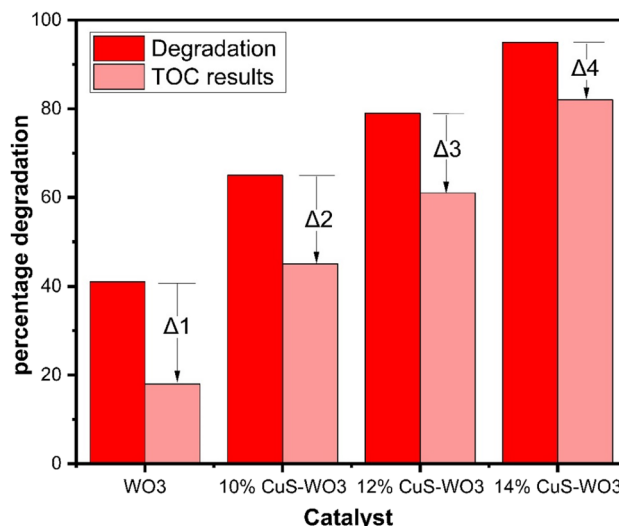


Fig. 9 Total organic carbon analysis to verify the percentage mineralization of RhB dye during photocatalytic treatment of wastewater using pure WO₃ and CuS:WO₃ composites

Table 3 Comparison of bandgap energy, degradation percentage and mineralization percentage by TOC for pure WO₃ and CuS:WO₃ nanocomposites

Sample	Band gap Energy (eV)	Degradation (%)	Mineralization or TOC (%)	Difference (Δ= degradation -TOC)%
WO ₃	2.61	41	18	23
10% CuS:WO ₃	2.47	65	45	20
12% CuS:WO ₃	2.38	79	61	18
14% CuS:WO ₃	2.25	95	82	13

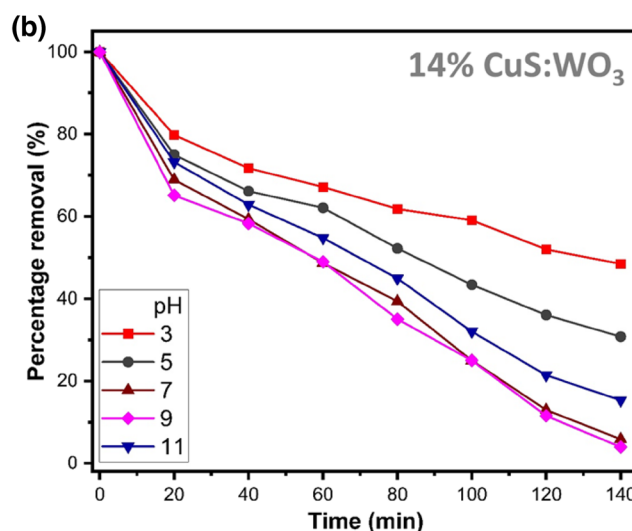
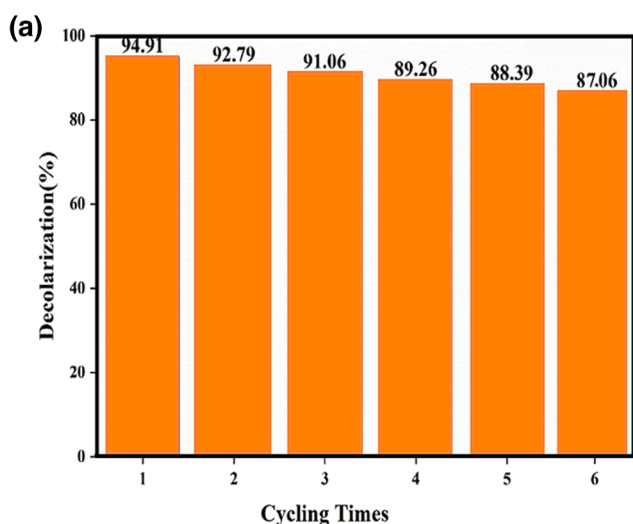
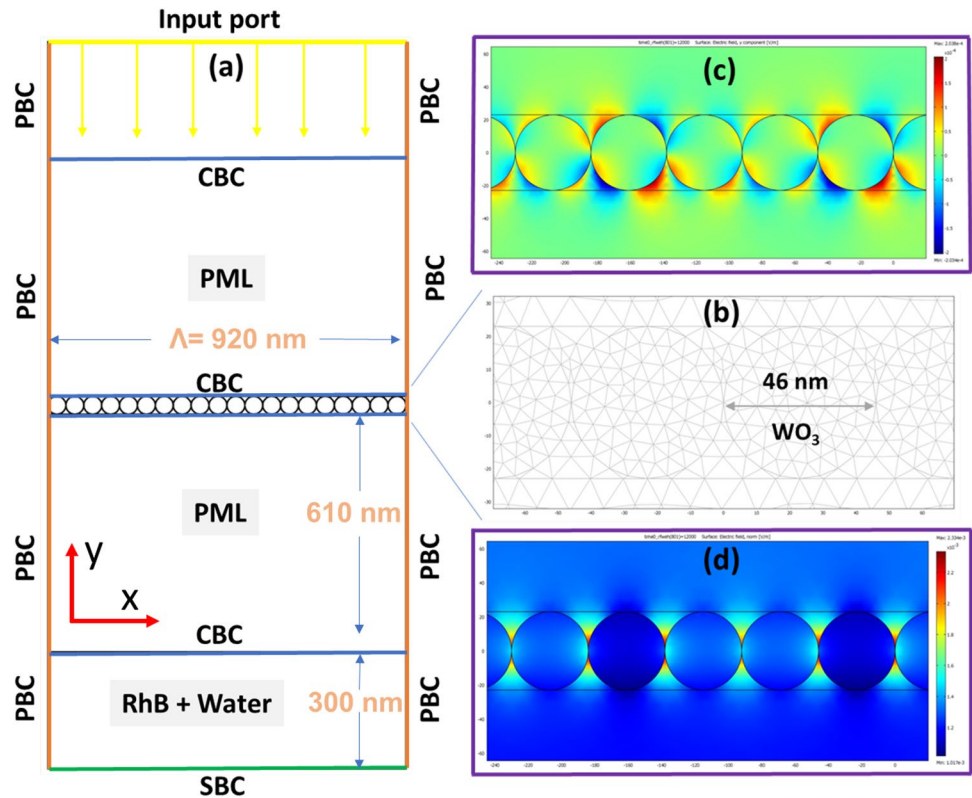


Fig. 8 a Reusability indicating to high photo-stability of the photo-catalyst for six cycles and b effect of pH for the degradation efficiency of best catalyst

Fig. 10 **a** Schematics of the 2D model, **b** meshed image of the model, **c** & **d** show the y-component and electric field norm respectively



Periodic boundary condition (PBC)

$$\mathbf{E}_{dst} = \mathbf{E}_{src} \exp(-j\mathbf{k} \cdot (\mathbf{r}_{dst} - \mathbf{r}_{src})) \quad (4)$$

Continuous boundary condition (CBC)

$$(\mathbf{n} \times (\mathbf{H}_1 - \mathbf{H}_2))_z = 0, (\mathbf{n} \times (\mathbf{E}_1 - \mathbf{E}_2))_z = 0 \quad (5)$$

Scattering boundary condition (SBC)

$$\mathbf{n} \times (\nabla \times \mathbf{A}_z) - jk\mathbf{A}_z = -jk(1 - \mathbf{k} \cdot \mathbf{n})\mathbf{A}_{0z} \exp(-j\mathbf{k} \cdot \mathbf{r}), \mathbf{A} = \mathbf{E} \text{ or } \mathbf{H} \quad (6)$$

Port

$$s = \int (\mathbf{E} - \mathbf{E}_1) \cdot \mathbf{E}_1 / \int \mathbf{E}_1 \cdot \mathbf{E}_1 \quad (7)$$

First, the model is meshed (Fig. 10b) and then normalized (Fig. 11a). The particle size of WO_3 used in the simulation was 46 nm (experimental value). The simulation is carried out for 200 min while WO_3 NPs were immersed in RhB and water solution. The wavelength is swept from 300 to 1000 nm with the step size of 1 nm for optimal results. TM polarized light has been used for the simulation. The Maxwell equations which govern the light matter interaction are given below (Eq. 8–10).

$$\nabla \times (\mu_r^{-1} \nabla \times \mathbf{E}) - \left(\epsilon_r - \frac{i\sigma}{\omega\epsilon_0} \right) k_0^2 \mathbf{E} = 0 \quad (8)$$

$$\nabla \times \left(\left(\epsilon_r - \frac{i\sigma}{\omega\epsilon_0} \right)^{-1} \nabla \times \mathbf{H} \right) - \mu_r k_0^2 \mathbf{H} = 0 \quad (9)$$

$$\mathbf{E} = E_z \mathbf{e}_z, \mathbf{H} = H_z \mathbf{e}_z, \epsilon_r = n^2 \quad (10)$$

Absorption, reflection and transmission was analyzed as shown in Fig. 11 c. It is observed that at any given wavelength, the following equation holds true (Eq. 11) which supports the argument that the model has been normalized correctly and no attenuation is present in the model.

$$I_{\text{reflection}} + I_{\text{absorption}} + I_{\text{transmission}} = 1 \quad (11)$$

After pure WO_3 , in order to simulate the nano-composites, a few atoms of WO_3 were replaced with CuS. Figure 10c & d shows the y-component of electric field and electric field norm for the simulated model. The results shown in Fig. 11b verifies the positive impact due to the presence of CuS for the absorption of light. Improved absorption attributes to the effective generation of photogenerated electron/hole pairs which leads to the higher photocatalytic efficiency. The same trend was obtained from the experiments.

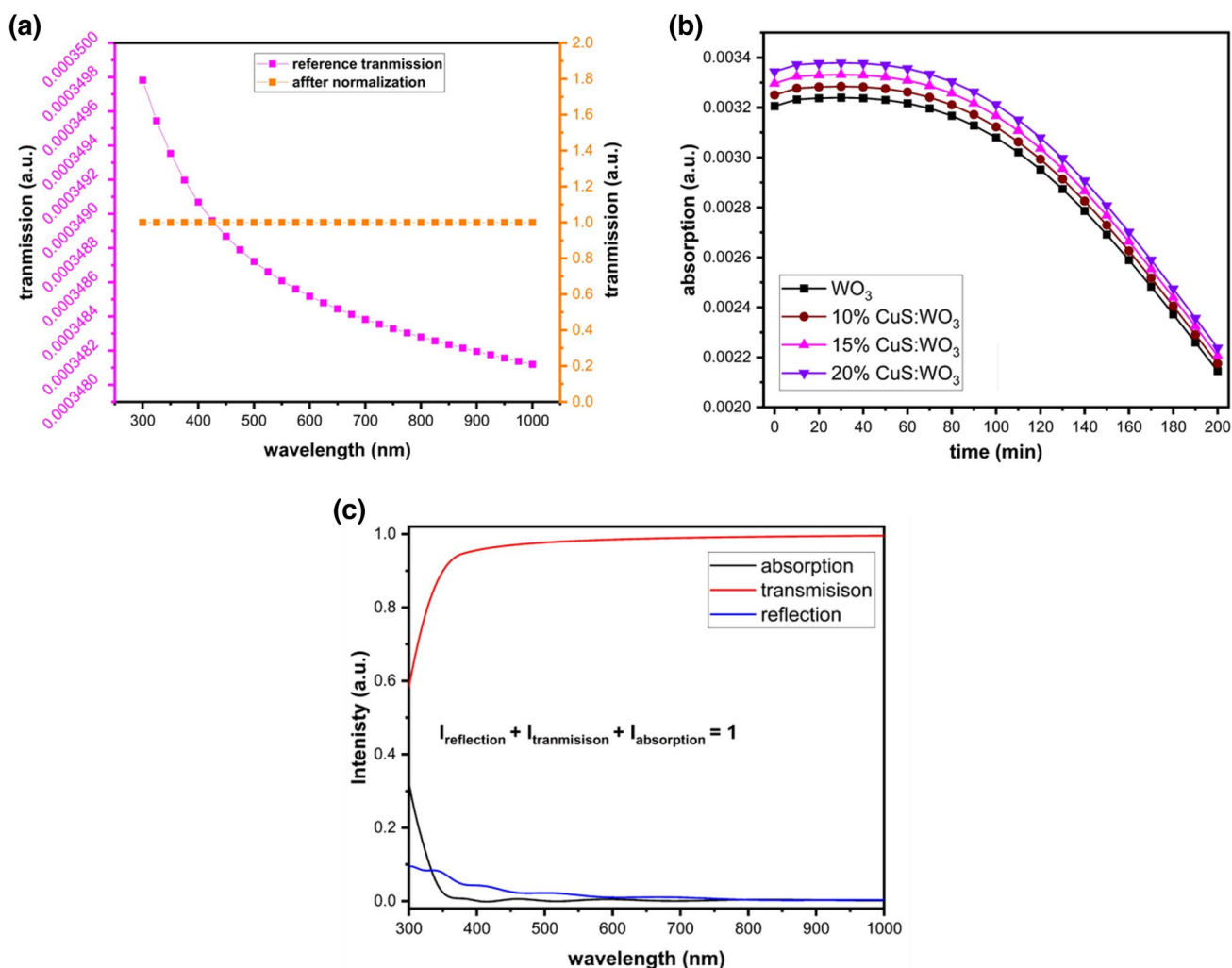


Fig. 11 **a** Normalization, **b** shows the improvement in absorption for incorporated samples as compared to pure WO_3 and **c** depicting absorption, reflection and transmission of the model when irradiated by TM polarized light

5 Conclusion

The XRD, UV–Vis SEM, EDX and PL Spectroscopic techniques were used to evaluate the structure, composition, morphological and optical parameters of synthesized nanocomposites. Degradation of RhB was used to analyze the photo-catalytic property samples under visible light photo-catalytic reaction. SEM depicted the nanorods morphology of CuS. Blend of Copper Sulfide and WO_3 introduces the lower band gap with the increased concentration of copper sulfide. The reduction in band gap from 2.61 to 2.25 eV produced defects and more ratio of copper sulfide decreases the crystalline form. This change would decrease the charge recombination rate and manifest the existence of copper sulfide. Dye degradation inferred that $\text{CuS}:\text{WO}_3$ nanocomposite manifest efficient photocatalytic behavior than pure WO_3 . Furthermore, degradation of organic pollutant (RhB) is accompanied by 14% CuS composite with

WO_3 catalyst. It degrades almost 94.9% of RhB dye in 140 min and it is just because in the composite, band gap and recombination rate is suppressed enhancing the degradation reaction rate of material. TOC analysis revealed that the rate of complete mineralization is less than the values observed by using UV–Visible spectrometer which attributes to the fact that decolorization of RhB dye may occur in initial few steps but complete deterioration of benzene ring is a multi-step reaction. Additionally, COMSOL is used to successfully correlate the experimental observations with simulation. Theoretical analysis verifies the enhanced absorption of light for nanocomposites as compared to pure WO_3 indicating the higher photocatalytic activity of nanocomposites for the degradation of organic contaminants. The promising results indicate that $\text{CuS}:\text{WO}_3$ composite is a potential catalyst for visible-light driven photocatalytic reactions for green energy applications as well as wastewater treatment.

Acknowledgements The Authors would like to thank Scientific Research Deanship at Ha'il University- Saudi Arabia for financial support of this project through Project Number RG-20119.

Author Contributions MA contributed towards conceptualization, methodology and initial draft. TI contributed in formal analysis, supervision and review of final draft whereas AM, NM, FIAA, WIE-S and SMM contributed for experimental investigation, formal analysis and validation. MA and MSM contributed for review and editing of final draft.

Funding Scientific Research Deanship at Ha'il University- Saudi Arabia, RG-20119

Data Availability All data generated or analyzed during this study are included in this published article

Declarations

Competing interests The Authors would like to thank Scientific Research Deanship at Ha'il University- Saudi Arabia for financial support of this project through Project Number RG-20119

Ethical Approval Not applicable.

Consent to Participate Not applicable.

Consent to Publish Not applicable.

References

1. A.A. Shah, A.D. Chandio, A.A. Sheikh, Boron doped ZnO nanostructures for photo degradation of methylene blue, methyl orange and rhodamine B. *J. Nanosci. Nanotechnol.* **21**(4), 2483–2494 (2021)
2. M.B. Tahir et al., WO₃ nanostructures-based photocatalyst approach towards degradation of RhB dye. *J. Inorg. Organomet. Polym Mater.* **28**(3), 1107–1113 (2018)
3. V. Dutta et al., An overview on WO₃ based photocatalyst for environmental remediation. *J. Environ. Chem. Eng.* **9**(1), 105018 (2021)
4. R. Ameta et al., Photocatalysis, in *Advanced oxidation processes for waste water treatment*. (Elsevier, Amsterdam, 2018), pp.135–175
5. C. Tanielian, Decatungstate photocatalysis. *Coord. Chem. Rev.* **178**, 1165–1181 (1998)
6. B. Chen et al., Preparation of MoS₂/TiO₂ based nanocomposites for photocatalysis and rechargeable batteries: progress, challenges, and perspective. *Nanoscale* **10**(1), 34–68 (2018)
7. M.A. Bhatti et al., Effective removal of methylene blue by surface alteration of TiO₂ with Ficus Carica leaf extract under visible light. *Nanomaterials* **12**(16), 2766 (2022)
8. M.A. Bhatti et al., Low temperature aqueous chemical growth method for the doping of W into ZnO nanostructures and their photocatalytic role in the degradation of methylene blue. *J. Clust. Sci.* (2022). <https://doi.org/10.1007/s10876-021-02069-6>
9. Y. Liu et al., One-step synthesis of a WO₃-CuS nanosheet hetero-junction with enhanced photocatalytic performance for methylene blue degradation and Cr (VI) reduction. *J. Chem. Technol. Biotechnol.* **95**(3), 665–674 (2020)
10. M. Sohaib et al., Novel sol-gel synthesis of Mo-doped ZnO-NPs for photo-catalytic waste water treatment using the RhB dye as a model pollutant. *Environ. Develop. Sustain.* (2022). <https://doi.org/10.1007/s10668-022-02543-9>
11. Z.A. Ujjan et al., Simultaneous doping of sulfur and chloride ions into ZnO nanorods for improved photocatalytic properties towards degradation of methylene blue. *Ceram. Int.* **48**(4), 5535–5545 (2022)
12. M.G. Peleyeju, E.L. Viljoen, WO₃-based catalysts for photocatalytic and photoelectrocatalytic removal of organic pollutants from water—A review. *J. Water Process Eng.* **40**, 101930 (2021)
13. A. Mehta et al., Band gap tuning and surface modification of carbon dots for sustainable environmental remediation and photocatalytic hydrogen production—A review. *J. Environ. Manage.* **250**, 109486 (2019)
14. M.A. Bhatti et al., Efficient photo catalysts based on silver doped ZnO nanorods for the photo degradation of methyl orange. *Ceram. Int.* **45**(17), 23289–23297 (2019)
15. C.D. SONG et al., Synthesis direct Z-scheme CuS-WO₃ photocatalysts based on an element-reaction route and their photocatalytic activity. *Acta Phys. Chim. Sin.* **33**(9), 1891–1897 (2017)
16. D. Rohilla et al., Microwave mediated synthesis of dopamine functionalized copper sulphide nanoparticles: an effective catalyst for visible light driven degradation of methylene blue dye. *Chemosphere* **277**, 130202 (2021)
17. F. Siddique et al., Effect of surface modification and H₂ reduction of WO₃ nanoparticles in methylene blue photodegradation. *Surf. Topogr. Metrol. Prop.* **8**(4), 045012 (2020)
18. T. Iqbal, M. Ashraf, A. Masood, Simple synthesis of WO₃ based activated carbon co-doped CuS composites for photocatalytic applications. *Inorg. Chem. Commun.* **139**, 109322 (2022)
19. C. Song et al., Enhanced performance of direct Z-scheme CuS-WO₃ system towards photocatalytic decomposition of organic pollutants under visible light. *Appl. Surf. Sci.* **425**, 788–795 (2017)
20. J. Khatter, R. Chauhan, Visible light-motivated photo-catalytic activity of CdS-Cu₉S₅ heterostructure for degradation of methylene blue. *Appl. Nanosci.* **12**(5), 1683–1696 (2022)
21. Y. Vyas et al., Biosynthesis and characterization of carbon quantum Dots@ CuS composite using water hyacinth leaves and its usage in photocatalytic dilapidation of brilliant green dye. *Mater. Chem. Phys.* **281**, 125921 (2022)
22. F. Peng et al., Gas sensing performance and mechanism of CuO (p)-WO₃ (n) composites to H₂S gas. *Nanomaterials* **10**(6), 1162 (2020)
23. A. Malathi, J. Madhavan, Synthesis and characterization of CuS/CdS photocatalyst with enhanced visible light-photocatalytic activity. *J. Nano Res.* (2017). <https://doi.org/10.4028/www.scientific.net/JNanoR.48.49>
24. J. Han et al., Mesoporous TiO₂ with WO₃ functioning as dopant and light-sensitizer: a highly efficient photocatalyst for degradation of organic compound. *J. Hazard. Mater.* **358**, 44–52 (2018)
25. P.S. Kumar, P.T. Ngueagni, A review on new aspects of lipopeptide biosurfactant: types, production, properties and its application in the bioremediation process. *J. Hazard. Mater.* **407**, 124827 (2021)
26. H. Song et al., Synthesis of Fe-doped WO₃ nanostructures with high visible-light-driven photocatalytic activities. *Appl. Catal. B* **166**, 112–120 (2015)
27. F. Stirling et al., Synthetic cassettes for pH-mediated sensing, counting, and containment. *Cell Rep.* (2020). <https://doi.org/10.1016/j.celrep.2020.02.033>
28. N.L. da Costa et al., Phosphotungstic acid on activated carbon: a remarkable catalyst for 5-hydroxymethylfurfural production. *Mol. Catal.* **500**, 111334 (2021)
29. X. Zhang et al., Construction of core-shell structured WO₃@SnS₂ hetero-junction as a direct Z-scheme photo-catalyst. *J. Colloid Interface Sci.* **554**, 229–238 (2019)

30. M. He et al., Highly sensitive and selective H₂S gas sensors based on flower-like WO₃/CuO composites operating at low/room temperature. *J. Alloy. Compd.* **788**, 36–43 (2019)
31. C. Wang et al., Preparation of Pd/PdO loaded WO₃ microspheres for H₂S detection. *Sens. Actuators, B Chem.* **321**, 128629 (2020)
32. H.-M. Lin et al., Nanocrystalline WO₃-based H₂S sensors. *Sens. Actuators, B Chem.* **22**(1), 63–68 (1994)
33. M. Punginsang et al., Selective H₂S gas sensors based on ohmic hetero-interface of Au-functionalized WO₃ nanowires. *Appl. Surf. Sci.* **571**, 151262 (2022)
34. B. Subash et al., Highly efficient, solar active, and reusable photocatalyst: Zr-loaded Ag–ZnO for reactive red 120 dye degradation with synergistic effect and dye-sensitized mechanism. *Langmuir* **29**(3), 939–949 (2013)
35. S. Kabcum et al., Ultra-responsive hydrogen gas sensors based on PdO nanoparticle-decorated WO₃ nanorods synthesized by precipitation and impregnation methods. *Sens. Actuators, B Chem.* **226**, 76–89 (2016)
36. Y. Zhang, J. Chang, Y. Wang, Mechanism analysis of PtPd-decorated hexagonal WO₃ nanorods for H₂S sensing application with ppt-level detection limit. *J. Alloy. Compd.* **892**, 162133 (2022)
37. A. Houas et al., Photocatalytic degradation pathway of methylene blue in water. *Appl. Catal. B* **31**(2), 145–157 (2001)
38. C.H. Kwon et al., Degradation of methylene blue via photocatalysis of titanium dioxide. *Mater. Chem. Phys.* **86**(1), 78–82 (2004)
39. S. Lakshmi, R. Renganathan, S. Fujita, Study on TiO₂-mediated photocatalytic degradation of methylene blue. *J. Photochem. Photobiol., A* **88**(2–3), 163–167 (1995)

Publisher's Note Springer Nature remains neutral with regard to jurisdictional claims in published maps and institutional affiliations.

Springer Nature or its licensor (e.g. a society or other partner) holds exclusive rights to this article under a publishing agreement with the author(s) or other rightsholder(s); author self-archiving of the accepted manuscript version of this article is solely governed by the terms of such publishing agreement and applicable law.